

Physics 411 Term Project:

Ben Rasmussen

December 12th, 2022

1 INTRODUCTION

The Vancouver Island School-based Weather Station Network is a web of weather stations set up on school campuses across Vancouver island. Developed by Andrew Weaver and Ed Wiebe associated with the University of Victoria, the network serves to gather meteorological data at many different geographic locations while involving the teachers and students in a meaningful way. This is motivated by a desire to expose learners and educators to the practical applications of Earth and Ocean Sciences. It has also gathered a large amount of data about the climate variables in the region.

In continuing with this mission, the data collected by this program is the focal point of the discussion presented here. Supplied with the temperature and pressure data of various stations around the southern island, we are able to complete a formal data analysis. The data sets used here are split into two distinct groups. The first consists of *minutely* sampled temperature and pressure for six different stations ranging from Cortes island all the way to the University of Victoria. As you can imagine, these are fairly substantial sets of data with an initial time of January 1st, 2016, continuing on to July 31st, 2022. The second set of time series' are *hourly* sampled in both temperature and pressure over the same period but for 15 different stations distributed on the island. This hourly data is the average of the temperature along the previous hour and then recorded.

In this document, a fairly comprehensive analysis of the provided data will be presented utilizing time series analysis techniques learned over the course of the semester. All calculations and data visualization was performed in a python Jupyter Notebook.

2 ANALYSIS TECHNIQUES

Here we will go over a brief introduction to a few of the techniques used to produce the plots in this paper. We begin first with the basic statistics of a time series.

2.1 Basic Statistics

All data sets used are assumed to be ergodic processes allowing us to make inferences about the statistics of the variables in smaller segment lengths. Our first statistic is simply the sample mean of a segment:

$$\bar{x} = \frac{1}{N} \sum_{i=1}^N x_i \quad (1)$$

We can use this to estimate the true parameter μ_x . To get an idea of variation in the data we then look to a sample variance given by the following expression:

$$s_x^2 = \frac{1}{N-1} \sum_{i=1}^N (x_i - \bar{x})^2 \quad (2)$$

This is the unbiased form of this estimate used to infer information about σ_x^2 . To perform confidence intervals for these values or another statistic such as a linear regression or slope calculation we can use the following form:

$$\mu_x (\text{or other quantity}) = \bar{x} \pm t_{\alpha/2,n} \cdot \frac{s_x}{\sqrt{N}} \quad (3)$$

For small samples we use the student-t distribution critical value, $t_{\alpha/2,n}$ as it approximates smaller statistics better than a normal distribution.

For a time series, it is of interest to create a function that measures the amplitude of correlation between either a time series with another or itself at

shifting levels of overlap. This is called the cross(or auto)- correlation function and it tells us how these time series will vary with respect to each other. In theory they are given by the following:

$$R_{xx} = E[x(t)x(t + \tau)] \quad (4)$$

$$R_{xy} = E[x(t)y(t + \tau)] \quad (5)$$

Where τ is the shifting lag between the time series'. In practice, we need to actually calculate this function. In a continuous regime this is given by:

$$R_{xy}(\tau) = \frac{1}{T - \tau} \int_0^{T - \tau} x(t)y(T + \tau)dt \quad (6)$$

Since most time series are not continuous, this can be extended to a discrete case:

$$R_{xy}(\tau) = \frac{1}{N - k} \sum_{i=1}^{N-k} (x_i \cdot y_{i+k}) \quad (7)$$

Where k is the index lag of a particular value of the function.

2.2 Not-So-Basic Statistics

2.2.1 Periodograms

To get a bit more involved in the analysis to find properties of a time series not immediately evident from plotting the function, we rely on more advanced techniques. If we wish to find the power associated with specific frequencies of oscillation in the frequency, such as daily fluctuations in temperature, we can consider the periodogram. The periodogram of a signal estimates the power spectral density of the frequencies present in that signal. Ideally the power spectrum is simply a form of the square modulus of the Fourier series of the signal.

$$\text{Periodogram : } \Gamma(f) = \frac{1}{T} |X(f)_m|^2 \quad (8)$$

In practice it is not so simple. In a discrete time series we can call on the welch method to find a good estimate for the power spectral density. We begin first with one realization of the periodogram for a discrete time series:

$$\Gamma(f_m) = \frac{\Delta t}{N} \left| \sum_{k=-n}^{n-1} x_k e^{-i2\pi f_m t_k} \right|^2 \quad (9)$$

This only gives on estimate for $\Gamma_1(f)$. To get the expected value we then use:

$$E[\Gamma(f)] = \lim_{M \rightarrow \infty} \frac{1}{M} \sum_{i=1}^M \Gamma_i(f) \quad (10)$$

We then need several realizations of this. But for a time series like changing time for a single station, we clearly can only have one realization. To circumvent this we can split the original time series in several subsections. If we get $M = NS$ different estimates, where NS is the number of segments we get $\Gamma_i(f)$ for every $i = 1, 2, \dots, NS$. The following expectation value is then:

$$\langle \Gamma(f) \rangle = \frac{1}{NS} \sum_{i=1}^{NS} \Gamma_i(f) \quad (11)$$

2.2.2 Scal(e)ograms

We can map the temporal changes in frequency power in two dimensions using continuous wavelet analysis. This is done with a continuous wavelet transform (CWT) on the data using different scaled forms of a mother wavelet. What we are returned with by using this analysis is the time-varying amplitude associated with the particular scaled wavelet and so must be plotted in 2D. Of course then the scaled wavelets will roughly correspond to frequency bands in the signal. The mother wavelet has the form:

$$g_{a,\tau} = \frac{1}{\sqrt{a}} g \left(\frac{t - \tau}{a} \right) \quad (12)$$

Performing a CWT on a signal has the following form:

$$X_g[\tau, a] = \frac{1}{\sqrt{a}} \int_{-\infty}^{\infty} g * \left(\frac{t - \tau}{a} \right) x(t) dt, \quad a = [0, \infty] \quad (13)$$

In this text, the mother wavelet used will be a Morlet wavelet. The expression defining the (non-complex) Morlet is as follows:

$$g(t) = e^{-\frac{1}{2}t^2} \sin(ct) \quad (14)$$

Or in the transform:

$$g_{a,\tau}(t) = \frac{1}{\sqrt{a}} e^{-\frac{1}{2}(\frac{t-\tau}{a})^2} \sin\left(c\frac{t-\tau}{a}\right) \quad (15)$$

2.2.3 Empirical Orthogonal Functions

Any data that varies in time or has multiple degrees of freedom can be decomposed into the dominant time varying amplitudes of the system. This is true for spatio-temporal varying data such as an irregular grid of temperature time-series. We can do this by computing the covariance matrix of all of the data arranged in a particular way and then computing the eigenvalue-eigenvector pairs of the matrix. We then assume that our covariance matrix can be written as:

$$z(x_m, y_m, t) = z_m(t) = \sum_{i=1}^M [a_i(t)\Phi_{i,m}] \quad (16)$$

Where M is the number of stations of data and $a_i(t)$ is the amplitude of the ith mode at a particular time. To do this analysis, it follows that the particular functions, $\Phi_{i,m}$, must be orthogonal such that:

$$\sum_{i=1}^M = (\Phi_{i,m}\Phi_{j,m}) = \delta_{ij} \quad (17)$$

Where δ_{ij} is the Kronecker delta. To solve for the various Φ s we must form the data covariance matrix.

$$\overline{z_m(t)z_k(t)} = \sum_{i=1}^M \sum_{j=1}^M [a_i(t)\Phi_{i,m}a_j(t)\Phi_{j,m}] \quad (18)$$

$$\overline{z_m(t)z_k(t)} = \sum_{i=1}^M \lambda_i \Phi_{i,m} \Phi_{i,k} \quad (19)$$

If we multiply this by the kth dominant eigenmode, $\Phi_{i,k}$, we can finally solve for each eigenvalue-vector pair:

$$\sum_{k=1}^M \overline{z_m(t)z_k(t)} \Phi_{i,k} = \sum_{k=1}^M \Phi_{i,k} \sum_{i=1}^M \lambda_i \Phi_{i,m} \Phi_{i,k} \quad (20)$$

Since we know that $\sum_{i=1}^M (\Phi_{i,m}\Phi_{i,K}) = \delta_{mk}$ we can finally solve for our eigenmodes or the empirical orthogonal functions using the final form of our solution:

$$\sum_{k=1}^M \overline{z_m(t)z_k(t)} \Phi_{i,k} = \lambda_i \Phi_{i,m} \quad (21)$$

The eigenvalue, λ_i is the variance associated with each mode while $\Phi_{i,m}$ is the ith spatial function with dominant EOFs determined by the magnitude of λ_i .

3 DATA VISUALIZATION

3.1 The Minute Data

As mentioned previously, the data collected each minute is distributed in six separate stations around the southern part of Vancouver Island. These data-sets, as expected, contain an enormous amount of minute-wise temperature and pressure data for the particular regions. We begin the analysis by first getting an intuition of where each station is situated with respect to the coastline of the island as can be seen below.

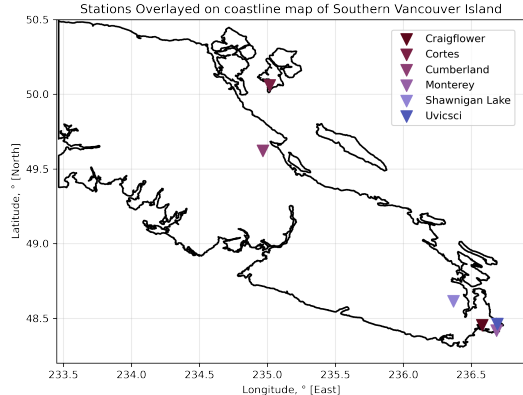


Figure 1: Locations of the six stations where minute data was collected

We can roughly split these six stations into two somewhat unique groups: those inside of the Capital Regional District [CRD] and those without. Although Shawnigan Lake is still near the major Metropolitan area we consider it outside along with Cortes island and the Cumberland station while Uvic Sci, Craigflower and Monterey are within.

3.1.1 A First Glance

The data-sets, as discussed, consist of 6+ years of temperature and pressure data that vary in time daily and seasonally. For temperature, we can notice this variation directly in the plot as follows.

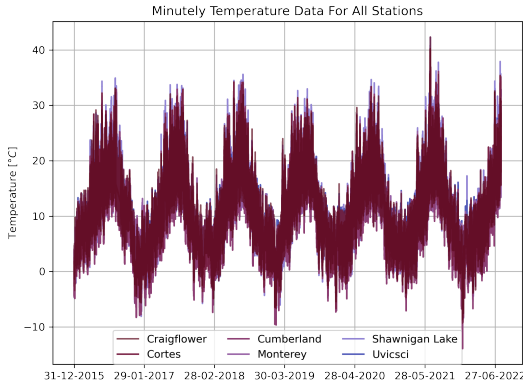


Figure 2: Temperature variation in time for all six minute data stations

From a first glance, there is clearly a dominant period corresponding to the yearly cycle. There is some deviation from station to station as seen in the fringes of the plot. It appears fairly regular with not much information initially apart from a few interesting features. The summer in 2021 stands out as an extreme outlier which is a result of the heat wave experienced by the island in July of the year. Conversely, the following winter, in 2022, there is a cold snap that also stands out. In a similar fashion, we can visualize the same time period in pressure variations.

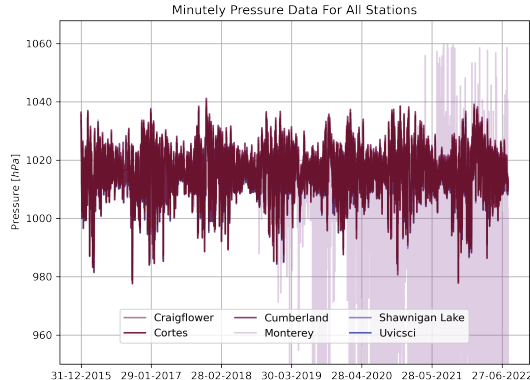


Figure 3: Pressure variation in time for all six minute data stations

Of note in this plot is the smaller variations from station to station in the pressure data. This suggests that the region containing all stations experience similar pressure system on order of larger areas than the region. This is true regardless of the forefront time series plotted. Of note is the weird behaviour in the Monterey pressure data. This author has no reasonable explanation for this response as Monterey lies in between other stations that do not experience this variability. As such, for the remainder of the analysis on this data, the Monterey pressure data will be ignored.

To adequately characterize these data-sets, it is useful to produce a probability density function for all instances of particular bins of temperature and pressure. We can infer both the distribution of the random variables in spread and in the centered value. Below, both the PDF of pressure and temperature can be found, separated into the three stations outside the CRD and those within it.

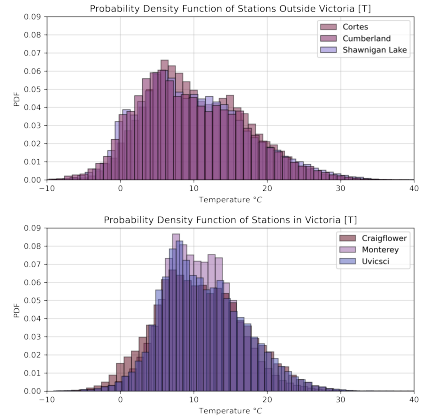


Figure 4: Probability Density Function for temperature distributions of the six minute stations. Separated for ease of comprehension into stations in the CRD and outside.

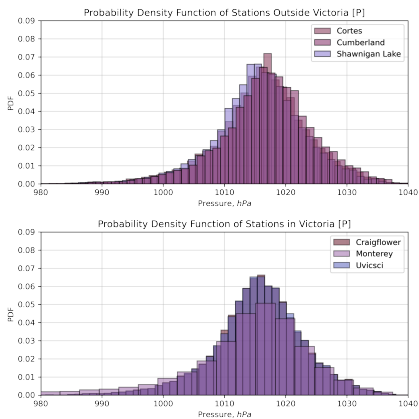


Figure 5: Probability Density Function for pressure distributions of the six minute stations. Separated for ease of comprehension into stations in the CRD and outside.

From the above, we are given our first opportunity to look at the behavioural differences between these two variables in the various regions. For the temperature PDF, we can notice a stark difference between the two categories. CRD stations exhibit a narrower distribution with a mean value $> 10^{\circ}\text{C}$ while non-CRD stations have a wider distribution with a mean that seems to fall below 10°C . Both of these density functions appear to be bimodal for almost all six station which likely is a result of the more extreme weather found in the summer and winter which can be seen temperature time series more pronounced peaks and valleys during those two seasons. It is reasonable to expect that the CRD stations would share characteristics, but it is interesting that even the Shawnigan Lake exhibits the non-CRD attributes, antithetical to total distance between each station.

As we have just proposed with pressure variation between stations, a similar acknowledgement can be made from the pressure PDF. Compared to the temperature density function, all six stations appear to match up much better in both center value and tails of the distributions. The CRD stations are slightly shifted to a lower center but all six stations seem to exhibit normal behaviour in their density functions, suggesting that pressure may be more randomly distributed when compared to temperature since large samples of randomly distributed random variables will approach a Gaussian. We also lack the bi-modality present in the temperature data.

3.1.2 Are Things Changing?

Although the data-sets only consist of six and a bit years worth of data, we can inquire whether the basic statistics of the system in consideration change throughout this time period. To do this, the naive method presented here considers the means and variances associated with each year of data for each station. From this, we can incidentally gain information about the station means in temperature and pressure as well as their associated variances and notice first order linear trends in this analysis. We begin with, largely the most important statistic, total mean temperature by year for the stations in consideration.

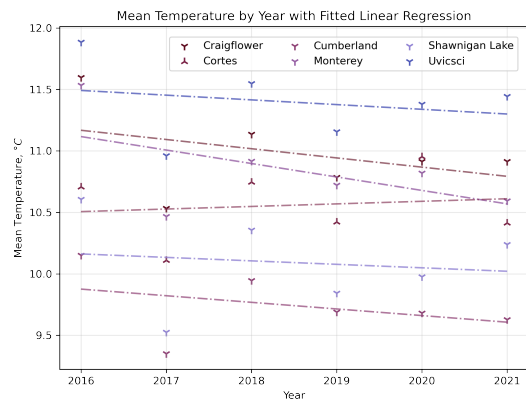


Figure 6: Yearly mean temperature values for the six stations with a linear regression applied to give idea of trend over the six years of data.

The mean temperature for all stations each year lie between 9 and 12°C . These means appear to vary in conjunction with each other which should be expected and will be discussed further. Of particular note is that five out of six of the stations all experience a decrease in mean temperature when fitted with a linear regression. This is largely unsurprising as 2016 was, across the board, a very warm year. Although not included in the plot above, the uncertainty associated with the linear regressions is large. All trends are not uniquely different from a stagnant temperature increase and so are not particularly insightful. A more complete analysis would separate seasonally to account for large difference that do not show up here and would also apply moving averages with respect to temperature evolution.

To a *very* first approximation, climate change is tied to the variance associated with the variables that make up a particular climate. We can then

consider the variance of these temperature time series yearly to inquire about this.

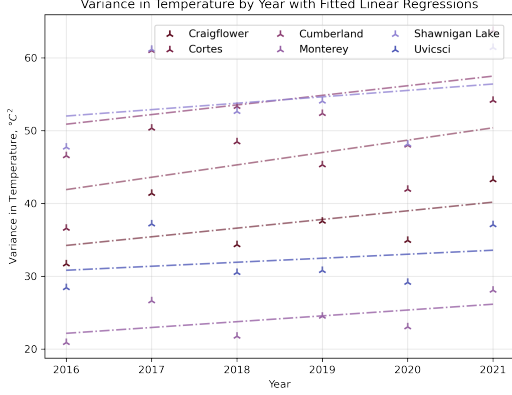


Figure 7: Yearly temperature variance associated with the six stations with a linear regression applied to give idea of trend over the six years of data.

In congruence with the means, the variances in each station follow similar trends with respect to the others. We can also notice that all six stations experience an increase in temperature variance as time goes on. This does hold up somewhat to a fit including uncertainty which was omitted for ease of comprehension.

We can do the exact same analysis on the pressure data to come to somewhat different conclusions.

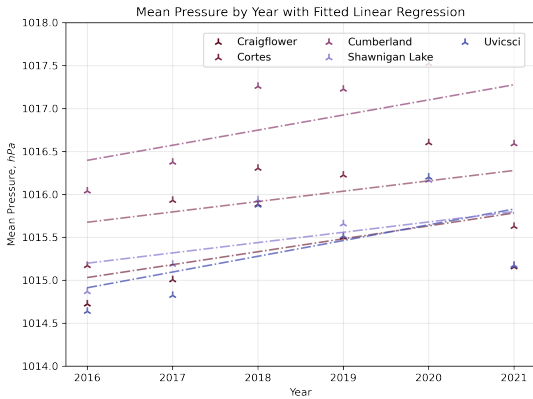


Figure 8: Yearly mean pressure values for the six stations with a linear regression applied to give idea of trend over the six years of data.

As experienced prior, variable means per year are a function of station and remain so here. The range that the pressure means change are very small and so not much can be gathered here. That being said, all five relevant stations experience an increase in pressure means as time continues. For the variance associated with pressure in each of these years, we can see that each year is tightly correlated by station but do not experience a noticeable trend. The variance associated with 2017 in pressure gives the impression of a negative correlation but within uncertainty this is not identically different from a positive trend.

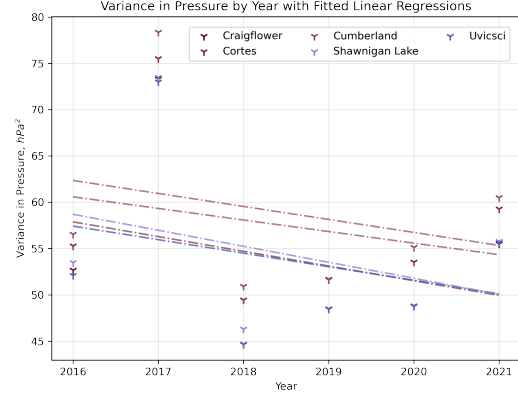


Figure 9: Yearly pressure variance associated with the six stations with a linear regression applied to give idea of trend over the six years of data.

3.1.3 What's in a Time Series?

To get intuition into the way that particular data-sets are related we can calculate a correlation function between them. In doing so, we can gain information about how a time series compares with respect to relative shifts in the other. We present here, both an auto- and cross-correlation function for both the most central CRD station, Uvic Sci, and the furthest station, Cortes. The data here has been smoothed using a moving average over each day. This is to eliminate the fluctuations inherent in the diurnal frequency band associated with only daily fluctuations.

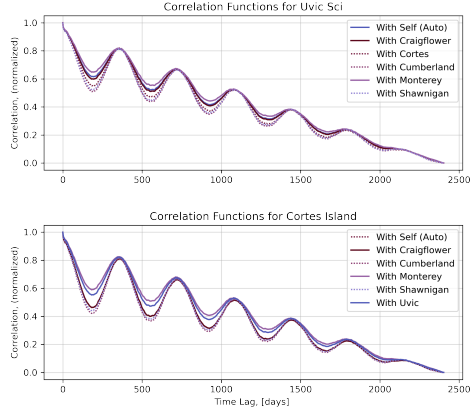


Figure 10: Auto and cross correlation functions for Uvic and the station further from Uvic, Cortes, over entire time series.

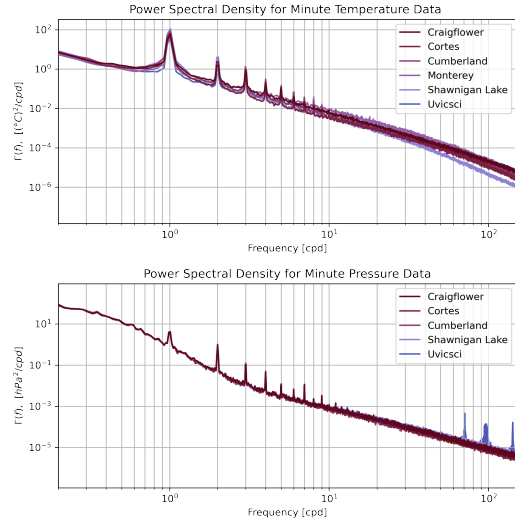


Figure 11: Power Spectral Density profiles for both temperature and pressure of all six minute data stations.

These plots contain a large amount of information. All cross correlation functions are nearly identically correlated at a zero-lag with an initial (small) steep drop off. After this, all functions, regardless of data-set pairs, experience a sinusoidal decay down to zero. We can interpret this as the frequency band associated with yearly oscillations. It is expected that the correlation between matched years is larger than if the time series were six months out of phase. There are a few interesting features of the data visualised above. For Uvic Sci, the time series most correlated with itself are the CRD stations (solid vs. dotted lines). This is not unexpected as they differ little spatially. What is odd is that for the Cortes island correlation functions, the most correlated stations are two of which that lie in the CRD and not without. This will hopefully be explained later by spatial distributions of dominant temperature modes.

We have had effects associated with both diurnal and yearly frequencies present in the data up until now. It is reasonable to then consider the power attributed to these bands. Using the Welch method for power will inevitably drown out the yearly period, but we can consider other contributions as shown in the following power spectral densities.

The calculations shown above include a power spectral density for both the temperature and pressure data for all relevant stations. We can gain further information about the time-series' by inspecting figure (11). Ignoring the curves and just considering the relative curves with respect to the stations, we can see that the temperature data power spectra differ from each other far more than the pressure data. This reinforces the propositions presented previously. The two spectra plots, however, both exhibit the same properties with slightly different results. As expected, much of the energy in both cases is tied to the diurnal band ($frequency = 10^0$). What is interesting is the considerable energy associated with the resonances of this frequency. Since we have taken the entire time series into consideration, higher order components should be expected, but this phenomena shows up nearly to the seventh and eighth order. This is a result of the deviation of the diurnal band from a pure sinusoid.

To further understand these time series', it is useful to consider the way that the spectrum evolves in time. In doing so, we can produce a spectrogram of the data. in this analysis, only the Uvic Sci will be considered for simplicity.

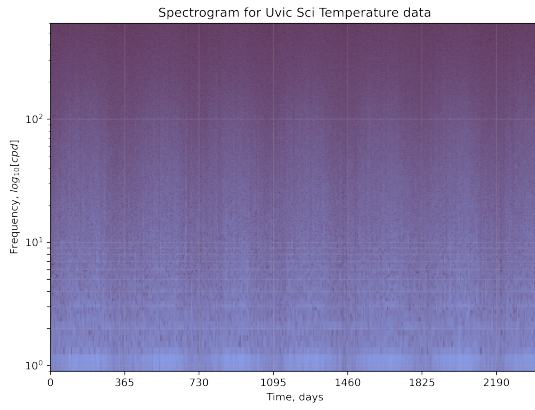


Figure 12: Spectrogram for the temperature data collected at the Uvic Sci station over entire time interval.

The information stored in the above plot is subtle. There is clearly dominance at the lower frequencies. The 'step-ladder' in the plot corresponds exactly to the resonances present in the power spectra. What is of particular interest is not the oscillations in the frequency axis but the variability in the time axis. The vertical grid lines are at yearly increments. This means that there is considerable more power (or variance) in the summer regions splitting the grid lines.

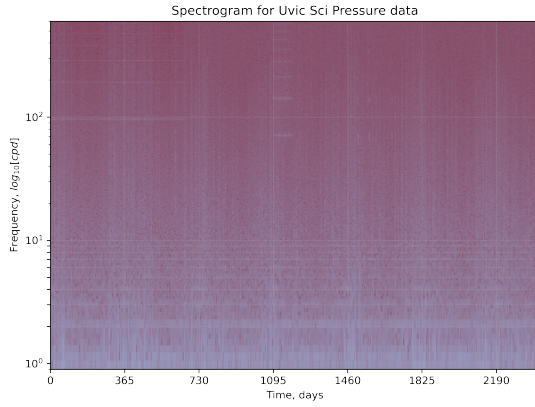


Figure 13: Spectrogram for the pressure data collected at the Uvic Sci station over entire time interval.

Conversely, the pressure spectrogram exhibits almost the opposite properties. There is certainly a 'ladder' type associated with figure (11) but the time oscillations in the plot line up with the minima in figure (12). We can infer information from

this; the temperature data has larger variance in the summer while the pressure data has larger variance in the winter.

3.2 The Hour Data

For the hour data we have over twice the amount of stations. Similar analysis to the above could be done but of more interest how a larger number of stations contribute to interpretations of the data spatially. Similar to the minute data, we begin by visualizing the relative positions of each station on the island.

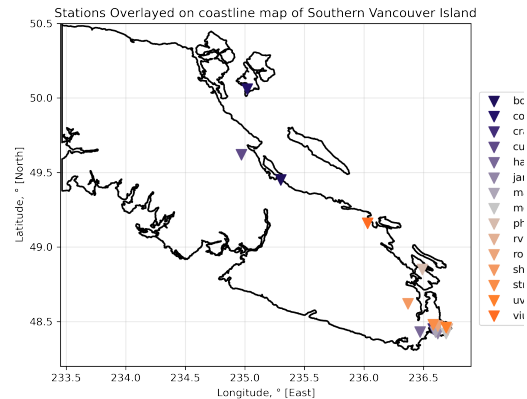


Figure 14: Locations of the fifteen stations where hourly data was collected.

3.2.1 A First Glance Pt. 2

It is always a good idea to reproduce a complete time series of the data to be analyzed before proceeding. As before, the time series for both temperature and pressure for the hour data are shown below.

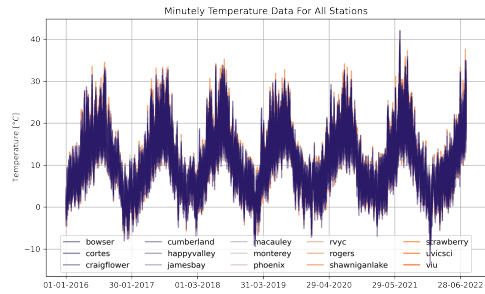


Figure 15: Temperature variation in time for all fifteen hour stations.

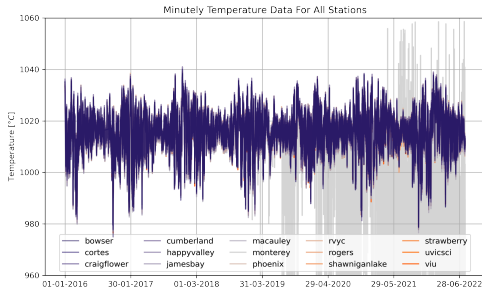


Figure 16: Pressure variation in time for all fifteen hour stations.

Once again, the same features are prevalent: larger variability per station in temperature versus pressure, a positive spike in 2021 and a negative spike in 2022, and an absolutely mangled pressure data-set for the Monterey data-set.

3.2.2 Space has 3 Dimensions

To get our bearings with respect to spatial data visuals, the mean data of the entire 6+ year data sets for each station is plotted below. A locally linear interpolation has been applied to extend into undefined regions.

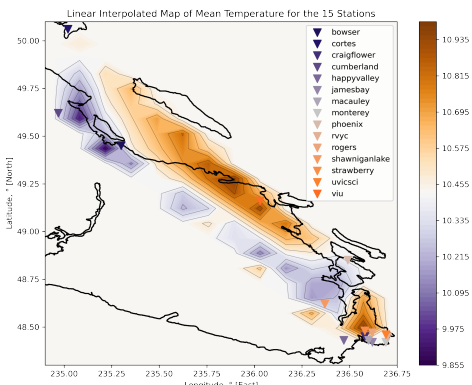


Figure 17: Mean Temperature Distribution for the entire data set, linearly interpolated spatially to include the means of all fifteen stations.

Using the same methodology present in figure (17), we now consider the mean temperature of each station year by year similar to what was done in figure (6). This allows us to gain information about

a reasonable distribution of temperatures in the region. Only the six complete years were considered in the plot below.

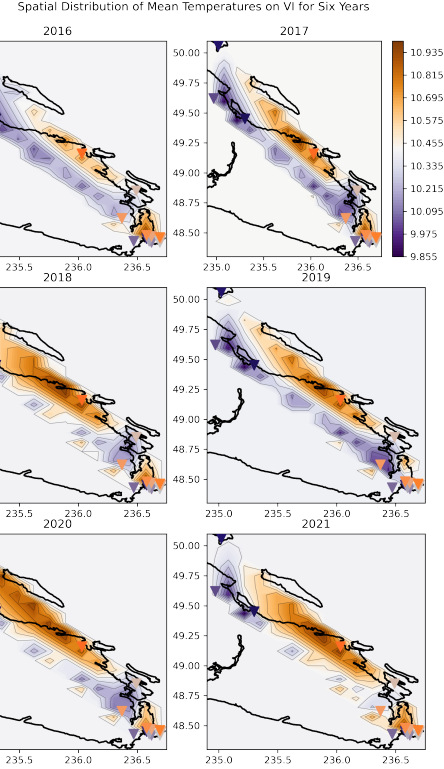


Figure 18: Mean Temperature distribution by year, linearly interpolated to include the means of all fifteen stations.

Although we are utilising large segments of the data, it is already clear that there is a noticeable pattern emerging in temperature distributions. The strait of Georgia following the North coast bounded by Texada Island seems to have a larger mean temperature in all years when compared to the inland region. Apart from maybe 2021, the coastal region included in the CRD is also warmer when compared to the inland regions.

Since space involves a third dimension, we can appropriately consider temperature variations with respect to elevation. Plotting the yearly mean temperature as a function of elevation for a year (example 2016) gives us the following plot.

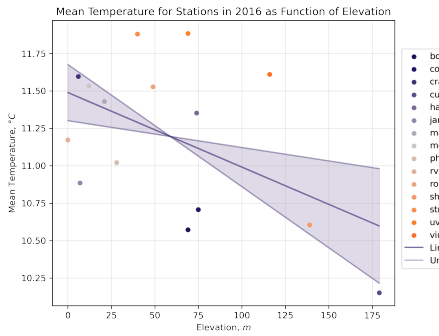


Figure 19: Mean Temperature of each station during the year 2016 as a function of elevation with a 95% confidence interval attached to the linear regression.

Within a 95% confidence level we achieve a negative correlation. For this particular year it is not unreasonable to conclude that as elevation increase, the region experiences lower and lower temperatures.

3.2.3 Eigenvector? I Barely Know Her

The spatial patterns of variability can be concisely reduced to a number of Empirical orthogonal functions. Using principle component analysis on the time series, we can project the dominant modes of variation into the spatial domain. We get these components from the eigenvalue-eigenvector pairs associated with the covariance matrix of our signals. In finding the first four dominant EOFs, we can compare them to the mean temperature spatial patterns found previously.

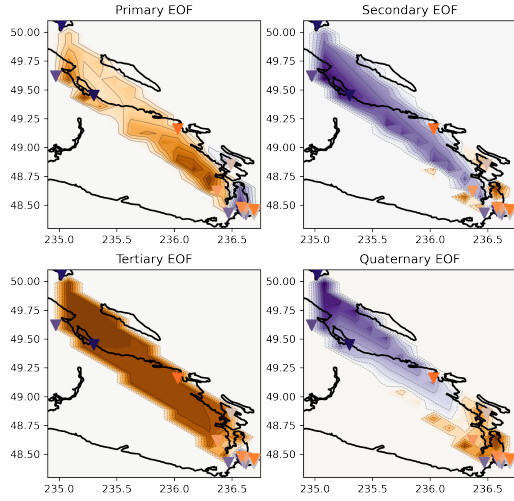


Figure 20: The first four dominant empirical orthogonal functions for mean temperature of the entire data set interpolated linearly.

The four components exhibit very different patterns in space and could reasonably make up much of the spatial varying time series with respect to all 15 stations. The primary mode makes up most of the baseline contributions with the lower temperature inland found in figure (18) coming from EOF 2. In the primary function the CRD is a lower temperature than in figure (17) and (18) but is made back up by the following three functions.

It is interesting to see how these functions dominate the entire system as a function of time. This will give information about the seasonality of the amplitudes of each mode.

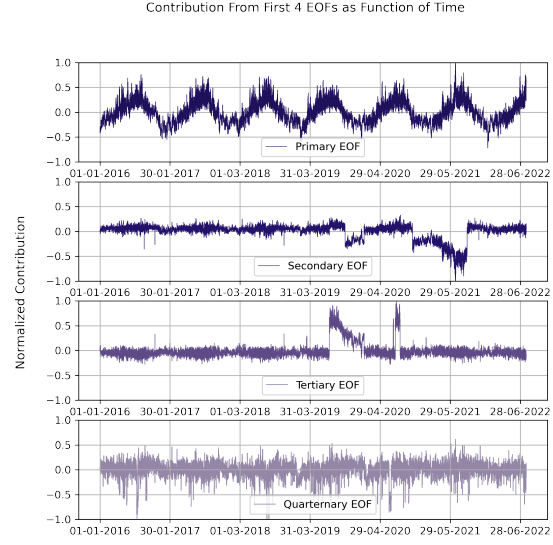


Figure 21: Temporal variation in relative dominance of the first four EOFs with respect to total variance contributions.

The primary mode clearly corresponds to summer increases in temperature almost perfectly. This is even more evident in the inclusion of both high amplitudes during the heatwave in 2021 and low amplitudes in the cold snap in 2022 mentioned previously. As for the second and third most dominant modes, there is certainly a modicum of seasonality. What is largely left unexplained is the weird behaviours in the second half of the time series in both cases. The fourth EOF seems to have ripples corresponding to the summer seasons combined with a large amount of noise.

We can also look into the total variance associated with each mode. The primary mode is certainly dominant with a fractional variance of 0.9029 while the following three most dominant EOFs have fractional variances of 0.0321, 0.0270, and 0.0116 respectively.

3.2.4 What Do You Call a Tiny Wave? *

As with the spectrogram for the minute data, it is interesting to see how a time series varies in frequency *in time*. To do this in another way we can take the continuous wavelet transform (CWT) of the signal. This somewhat ambiguously gives us the desired information about the signal. The following plots will all be done using a Morlet wave as the mother wavelet with only the Uvic Sci data.

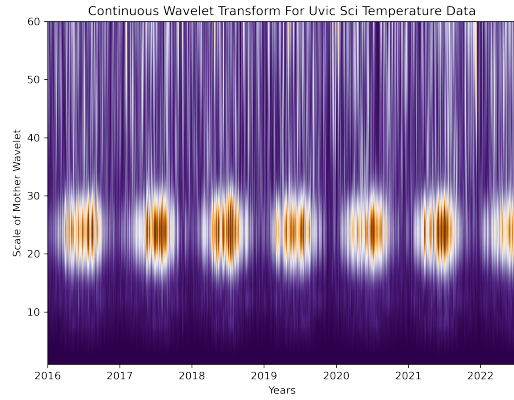


Figure 22: Continuous wavelet analysis applied to the Uvic Sci station time series of hourly sampled temperature data.

Since we do not know the exact parameters the scaling corresponds to from first glance, it is reasonable to assume from the spectrogram produced earlier that the dominant fluctuations seen above come from daily oscillations. We can see that these fluctuations appear only in the summer periods. There is some power, and noise, in higher scales of the mother wavelet but it is clearly overpowered by the leading signal.

once again, the pressure data exhibits something wholly different. Much of the dominate scales occur much after the temperature set. These also correspond to the winter season rather than the summer like in the temperature set. This once again suggests that there is more variance and power in the winter months for pressure and more power in the summer months for temperature.

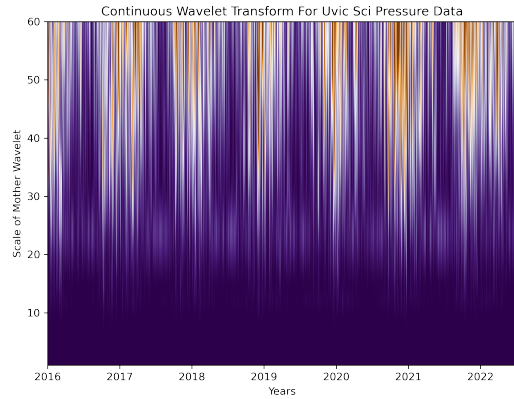


Figure 23: Continuous wavelet analysis applied to the Uvic Sci station time series of hourly sampled pressure data.

To demonstrate how the wavelet transform is unstable for small time series with little to no dominant frequencies, a plot of a Morlet CWT for the Uvic Sci data on this author’s birthday in 2020 is included below. This is here largely because it looks like perfectly cooked marsh-mallows.

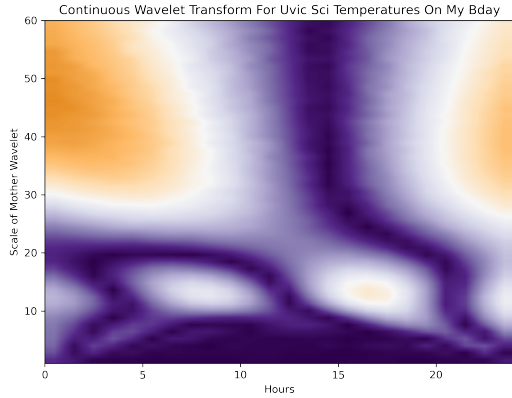


Figure 24: Continuous wavelet analysis applied to the Uvic Sci station time series of hourly sampled temperature data on my birthday in 2020

* A Microwave

3.2.5 Life’s a Beach

To conclude our analysis on the data, we wish to visualise the data in such a way as to truncate the plotted heat maps by the coastline or beaches surrounding the island. This serves to better match up with the Vancouver Island School-based Weather Station network presentation of the spatial distribution of temperature. We present this in two forms. The first as a recreation of figure (17) bounded by the coastline with a higher order interpolation as seen below. This is entire time series inclusive for mean temperatures.

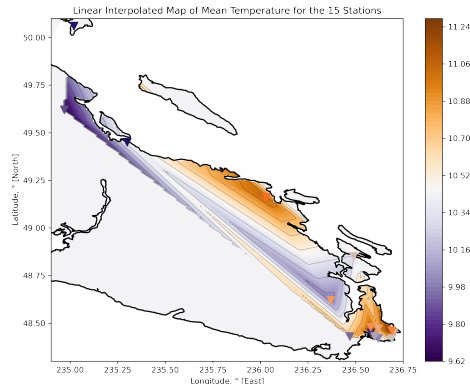


Figure 25: Entire data set mean temperature interpolation truncated by coastline.

Since this visualization strategy lends itself to daily temperature distributions, we also present an inverse squared interpolated map of the temperature profile only on this author’s birthday in 2020.

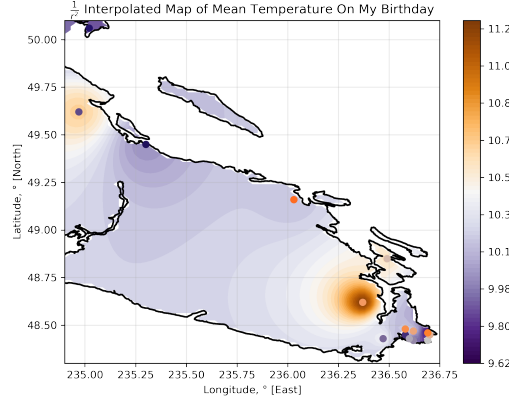


Figure 26: Mean temperature with a $\frac{1}{r^2}$ interpolation applied truncated by coastline on my birthday in 2020

And with that, our analysis on these data sets is concluded. It has been shown that there is clear seasonal patterns with respect to variance and dominant patterns in the system in the form of the periodogram and scaleogram. The dominant empirical orthogonal functions were extracted from the spatio-temporal temperature distribution of the 15 stations and were plotted in time with respect to their relative contributions. We also saw that there was predictable spatial patterns in temperature means by

year with inland areas experiencing, on the whole, lower temperatures when compared to stations along the Strait of Georgia. The increase in temperature over the six years was left ambiguous while variance

seemed to increase. For pressure, the opposite was true. It was also found that there was a non-negligible downward trend in mean temperature as a function of elevation.

Acknowledgements

The data used in this analysis was acquired from the Vancouver Island School-Based Weather Station Network (VISN) facilitated by Andrew Weaver and Ed Wiebe, both faculty at the University of Victoria and was provided here by Professor Johannes Gemmrich. The notes used to produce the analysis techniques section were all provided by the wonderful Dr. Gemmrich who was an excellent professor for the semester. For that I give him my thanks.